

ADDRESSING DIVERGENT REPRESENTATIONS FROM CAUSAL INTERVENTIONS ON NEURAL NETWORKS

Satchel Grant ^{*†‡} Simon Jerome Han ^{*‡} Alexa R. Tartaglini ^{†‡} Christopher Potts ^{§†‡}

ABSTRACT

A common approach to mechanistic interpretability is to causally manipulate model representations via targeted interventions in order to understand what those representations encode. Here we ask whether such interventions create out-of-distribution (divergent) representations, and whether this raises concerns about how faithful their resulting explanations are to the target model in its natural state. First, we demonstrate empirically that common causal intervention techniques often do shift internal representations away from the natural distribution of the target model. Then, we provide a theoretical analysis of two classes of such divergences: ‘harmless’ divergences that occur in the null-space of the weights and from covariance within behavioral decision boundaries, and ‘pernicious’ divergences that activate hidden network pathways and cause dormant behavioral changes. Finally, in an effort to mitigate the pernicious cases, we modify the Counterfactual Latent (CL) loss from Grant (2025) that regularizes interventions to remain closer to the natural distributions, reducing the likelihood of harmful divergences while preserving the interpretive power of interventions. Together, these results highlight a path towards more reliable interpretability methods.

1 INTRODUCTION

A central goal of mechanistic interpretability is to understand what the internal representations of neural networks (NNs) encode and how this gives rise to their behavior. Perhaps the most powerful approach to pursuing this goal is through causal interventions, where methods such as activation patching and Distributed Alignment Search (DAS) directly manipulate internal representations to test how they affect downstream outputs (Geiger et al., 2021; 2023; Wu et al., 2023; Wang et al., 2022; Meng et al., 2023; Nanda, 2022; Csordás et al., 2024). Indeed, even correlational interpretability methods such as Sparse Autoencoders (SAEs) and Principal Component Analysis (PCA) often use causal interventions as a final judge for whether the features they identify are truly meaningful (Huang et al., 2024; Dai et al., 2024). Causal interventions thus occupy a central place in making functional claims about neural circuitry (Pearl, 2010; Geiger et al., 2024; 2025; Lampinen et al., 2025; Braun et al., 2025).

The use of causal interventions for mechanistic interpretability rests upon a fundamental assumption that counterfactual model states created by interventions are realistic for the target model. Despite its pervasiveness, however, this assumption is often untested. For example, some activation patching experiments multiply feature values by up to 15x (Lindsey et al., 2025); in these settings, it seems possible that intervened representations diverge significantly from the NN’s natural distributions. This raises questions about the reliability of causal interventions for mechanistic interpretability. Do divergent representations change what an intervention can say about an NN’s original mechanisms? When, and to what extent, is it okay for such divergences to occur? When it is not okay, how can we prevent them from occurring?

In this work, we provide both empirical and theoretical insight on these issues. We first demonstrate that divergent representations are a common issue for causal interventions – across a wide range of intervention methods, we find that intervened representations often do diverge from the

^{*}Department of Psychology

[†]Department of Computer Science

[‡]{grantsrb, sjeromeh, alexart, cgpotts}@stanford.edu

[§]Department of Linguistics

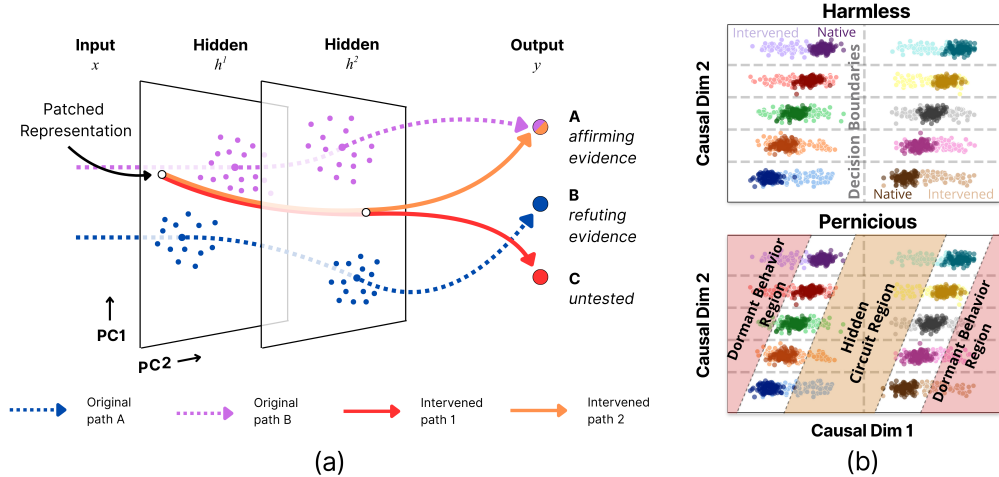


Figure 1: Causal interventions can recruit hidden circuits that produce misleadingly confirmatory or dormant behavior. (a) For example, consider original pathways (dashed arrows) for two classes A and B that naturally carry activity to different behavioral outputs y . In a hypothetical intervention meant to find path A, patching h^1 with a divergent representation can activate distinct, hidden pathways (solid arrows) that result in misleadingly confirmatory behavior (orange) and/or undetected behavior (red). (b) Now consider 2D projections of the neural activity of h^1 for a different network that classifies states into one of 10 classes (denoted by hue). Suppose that natural representations (dark points) lie within well-defined decision boundaries (dashed lines) and covary along causal axes, and that intervened representations (light points) are constructed by patching the first axis from a sampled natural representation. Although these representations diverge from the native distribution, this can be harmless (top) or pernicious (bottom) depending on the network’s functional landscape. In particular, it can be pernicious if the network has a functional landscape where intervened activity may unknowingly recruit hidden circuits (visualized as an orange region) or cross dormant behavioral boundaries (red regions).

target NN’s natural distribution. We then provide theoretical examples of two types of divergent representations: ‘harmless’ divergences that can occur from within-decision-boundary covariance along causal dimensions or from deviations along the null-space of the NN layers, which can even be desirable for some mechanistic claims, and ‘pernicious’ divergences that activate hidden network pathways and can cause dormant changes to behavior. We provide discussion on how the harmless and pernicious cases are not always mutually exclusive, where the harm often depends on the specific mechanistic claims. Finally, we provide a broad-stroke, initial solution for mitigating pernicious divergences by minimizing all divergences along causal subspaces (as discovered by DAS). This solution consists of a modified version of the Counterfactual Latent (CL) loss introduced in [Grant \(2025\)](#) applied to constrain intervened representations along causal dimensions. We confirm its promise by showing that it can improve out-of-distribution (OOD) performance on interventions in synthetic tasks. Although we do not propose this method as the final solution to representational divergence, we pose it as a step towards more reliable interventions. Our contributions are as follows.

1. We show empirical examples of divergence between natural and causally intervened representations for a variety of causal methods (Section 3).
2. We provide a theoretical treatment of cases in which divergent representations can arise innocuously from variation along null-space directions and from covariance within decision boundaries of behavioral subspaces, demonstrating that some types of divergence can be okay and even desired (Section 4.1)
3. We provide synthetic examples of cases where divergent representations can (1) activate hidden, non-native computational pathways while still resulting in hypothesis-affirming behavior, and (2) cause undetected, latent behavioral changes, together raising questions about the mechanistic claims that can be made from patching results alone (Section 4.2).
4. We adapt the CL loss from [Grant \(2025\)](#) by averaging over vector labels and exclusively minimizing divergence along causal dimensions. We then use this adapted CL loss to improve

OOD performance on causal interventions, providing an initial path towards reducing pernicious divergences (Section 5).

2 BACKGROUND AND RELATED WORK

2.1 ACTIVATION PATCHING

Activation patching generally refers to a process of “patching” (i.e. substituting) some portion of neural activity at an intermediate layer into or from a corrupted forward pass of a network (Geiger et al., 2020; Vig et al., 2020; Wang et al., 2022; Meng et al., 2023; Zhang & Nanda, 2024). It can be performed at various granularities such as whole layers, attention heads, or individual neurons. Many forms of activation patching can be unified under the assumption that subspaces, rather than individual neurons, are the atomic units of NN representations (Rumelhart et al., 1986; McClelland et al., 1986; Smolensky, 1988; Elhage et al., 2022; Geiger et al., 2021; Grant et al., 2024). Activation patching at the level of individual neurons can be understood as subspace patching along neuronal axes, and many of its high-level granularities can be understood as specific forms of individual neuron patching (Geiger et al., 2020; Vig et al., 2020; Wang et al., 2022; Meng et al., 2023).

2.2 DISTRIBUTED ALIGNMENT SEARCH

Distributed Alignment Search (DAS) (Geiger et al., 2021; 2023; Wu et al., 2023) can be understood as a form of activation patching that operates in a transformed basis so that specific, causally relevant subspaces can be manipulated analogously to high-level variables from causal abstractions (CAs) (e.g. symbolic programs). Many cases of individual neuron patching can be understood as a specific case of DAS that uses the identity transform. We use DAS throughout Sections 4 and 5, so here we introduce its theory and background.

DAS is a general framework for finding alignments between subspaces within an NN’s latent vectors and variables from causal abstractions (CAs). DAS achieves this by testing the hypothesis that an NN’s latent state vector $h \in R^{d_m}$ can be transformed into a vector $z \in R^{d_m}$ that consists of orthogonal subspaces encoding interpretable variables from CAs. This transformation is performed by a learnable, invertible *Alignment Function* (AF), $z = \mathcal{A}(h)$. We restrict our considerations to orthogonal AFs of the form $\mathcal{A}(h) = Qh$ where $Q \in R^{d_m \times d_m}$ is an orthogonal matrix, but AFs can in principle take many forms (Grant et al., 2024; Sutter et al., 2025). This transformation allows us to formulate h in terms of interpretable variables and to manipulate individual variable values.

For a given CA with variables $\text{var}_i \in \{\text{var}_1, \text{var}_2, \dots, \text{var}_n\}$, DAS tests the hypothesis that z is composed of subspaces $\vec{z}_{\text{var}_i} \in R^{d_{\text{var}_i}}$ corresponding to each of the variables from the CA. A causally irrelevant subspace $\vec{z}_{\text{extra}} \in R^{d_{\text{extra}}}$ is also included to encode extraneous, functionally irrelevant activity (i.e., the behavioral null-space).

$$\mathcal{A}(h) = z = \begin{bmatrix} \vec{z}_{\text{var}_1} \\ \vec{z}_{\text{var}_2} \\ \vdots \\ \vec{z}_{\text{var}_n} \\ \vec{z}_{\text{extra}} \end{bmatrix} \quad (1)$$

Here, each $\vec{z}_{\text{var}_i} \in R^{d_{\text{var}_i}}$ is a column vector of potentially different lengths, where d_{var_i} is the *subspace size* of var_i , and all subspace sizes satisfy $d_{\text{extra}} + \sum_{i=1}^n d_{\text{var}_i} = d_m$. The value of a single causal variable encoded in h can be manipulated through an interchange intervention defined as follows:

$$\hat{h} = \mathcal{A}^{-1}((\mathcal{I} - D_{\text{var}_i})\mathcal{A}(h^{\text{trg}}) + D_{\text{var}_i}\mathcal{A}(h^{\text{src}})) \quad (2)$$

Here, $D_{\text{var}} \in R^{d_m \times d_m}$ is a manually defined, block diagonal, binary matrix that defines the subspace size d_{var_i} , and $\mathcal{I} \in R^{d_m \times d_m}$ is the identity matrix. Each D_{var_i} has a set of d_{var_i} contiguous ones along its diagonal to isolate the dimensions that make up \vec{z}_{var_i} . h^{src} is the *source vector* from which the subspace activity is harvested, h^{trg} is the *target vector* into which the harvested activity is patched, and \hat{h} is the resulting intervened vector that replaces h^{trg} in the model’s processing. This allows the model to make predictions using a new value of variable var_i .

To train \mathcal{A} , DAS uses *counterfactual behavior* $c \sim \mathcal{D}$ as training labels, where c is generated from the CA. c , for a given state of a CA and its context, is the behavior that would have occurred had

a causal variable taken a different value and everything else remained the same. c is generated by freezing the state of the environment, changing one or more variable values in the CA, and using the CA to generate new behavior in the same environment using the new values. We train \mathcal{A} on intervention samples while keeping the model parameters frozen, minimizing the following objective (for non-sequence-based settings):

$$\mathcal{L}_{\text{DAS}}(\mathcal{A}) = -\frac{1}{N} \sum_{k=1}^N \log p_{\mathcal{A}}(c^{(k)} \mid x^{(k)}, \hat{h}^{(k)}), \quad (3)$$

where N is the number of samples in the dataset, $c^{(k)}$ is the counterfactual label in sample k , $x^{(k)}$ is the model input data, and $p_{\mathcal{A}}(\cdot \mid \cdot)$ is the model’s conditional probability distribution given the intervened latent vector, \hat{h} . We minimize $\mathcal{L}_{\text{DAS}}(\mathcal{A})$ using gradient descent, backpropagating into \mathcal{A} with all model weights frozen. \mathcal{A} is evaluated on new intervention data, where the model’s accuracy on c following each intervention is referred to as the Interchange Intervention Accuracy (IIA).

2.3 PROBLEMATIC CAUSAL INTERVENTIONS

Prior work has implicitly explored issues related to representational divergence from causal interventions. For example, methods such as causal scrubbing or noising/denoising activation patching (Wang et al., 2022; LawrenceC et al., 2022; Meng et al., 2023; Chen et al., 2025; Zhang & Nanda, 2024) intentionally introduce divergent representations to test the sufficiency, completeness, and faithfulness of proposed circuits. Works such as Wattenberg & Viégas (2024), Méloux et al. (2024), and Chen et al. (2025) also implicitly explore the dangers of divergent intervened representations by showing how circuits and features can be redundant or have combinatorial effects that are difficult to enumerate given current methodologies, while Zhang & Nanda (2024) and Heimersheim & Nanda (2024) point out easy misinterpretations of patching results. Shi et al. (2024) and Wang et al. (2022) provide criteria centered on faithfulness, completeness, and minimality for evaluating circuits through causal interventions. A body of work on counterfactual explanations exists, some of which has explored differences between on-manifold and off-manifold adversarial attacks (Stutz et al., 2019), and some works have explored constraining counterfactual features to the manifold of the dataset (Verma et al., 2024; Tsiorvas et al., 2024). Our proposed method in Section 5 differs in that it trains a principled alignment to generate counterfactual representations and it constrains deviations along causal dimensions. For DAS in particular, Makelov et al. (2023) demonstrate that it is possible to produce an interaction between the null-space and dormant subspaces that affect behavior. Because they define dormant subspaces as those that do not vary across different model inputs, variation along these directions is, by definition, a form of divergent representation. Finally, Sutter et al. (2025) posit that it is possible to align any causal abstraction to NNs under a number of assumptions including a sufficiently powered, non-linear alignment function, raising questions about what non-linear causal interventions really tell us.

3 ARE DIVERGENT REPRESENTATIONS A COMMON PHENOMENON?

Here we empirically demonstrate how common interpretability methods such as mean difference vector patching (Feng & Steinhardt, 2024), Sparse AutoEncoders (SAEs) (Bloom et al., 2024), and DAS can result in representations that diverge from the original distribution. The possibility of representational divergence has also been indirectly explored through attention patterns in cases of activation patching that use Gaussian noise corruption (Zhang & Nanda, 2024). Figure 2 shows the top two principal components of the original and intervened latent vectors, distinguished by color. These results show that divergence is a common phenomenon in practice and is not specific to any one method. Even simple methods that patch along a single, mean direction are subject to divergence, despite high behavioral accuracy (Feng & Steinhardt, 2024; Geiger et al., 2023). We quantify this divergence in Figure 2(a) by computing Earth Mover’s Distance (EMD) (Villani, 2009) between all components of the original and intervened activity, and then subtracting a baseline EMD of the original activity compared against itself. See Appendix A.1 for details. Note that these panels do not necessarily imply that the respective methods are invalid or that the claims of the papers are incorrect – this depends on the specific causal claims being made, and we next explore ways in which divergence can be pernicious or harmless to these claims.

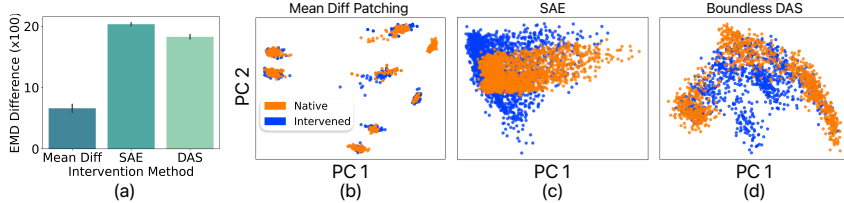


Figure 2: **Representational divergence is a common issue across various forms of patching.** (a) Shows the difference in Earth Mover’s Distance (EMD) between natural compared to intervened latent states and natural latent states compared to themselves. (b)-(d) scatter plots show the top two principal components of natural latent states (orange) and corresponding intervened latent states (blue). All are taken from the transformer residual stream at the intervention positions, and PCA is performed over the combined set of native and intervened latent vectors. Specifically, (b) shows the natural and intervened residual stream from a single layer taken from interventions replicating the results of Feng & Steinhardt (2024) who add and subtract intervention vectors computed as the mean difference between two binding states, (c) shows original vectors and the SAE reconstructed vectors for a single transformer layer using SAELens (Bloom et al., 2024), and (d) shows projected latent states from before and after interchange interventions for Boundless DAS (Wu et al., 2023).

4 WHEN ARE DIVERGENT REPRESENTATIONS HARMLESS OR PERNICIOUS?

4.1 HARMLESS CASES

We first explore cases in which we might consider divergent representations to be harmless to many general computational claims. First among these is a set of cases in which divergence is bottlenecked into the null-space of the next computational layer(s). One could even desire to intervene along this subspace as a causal test to demonstrate that such dimensions are indeed in the null-space. These dimensions can be, for example, the null-space of all subsequent weight matrices, or the space of all negative numbers before a ReLU nonlinearity. If one cares only about the model’s output behavior, any divergence that has no effect on the model’s behavior would therefore be innocuous. Indeed, this covers many present day scenarios. However, it is difficult to define the full behavioral null-space in practice, due to the possibility of dormant behavioral changes, which we discuss in Section 4.2.2.

A less obvious case of harmless divergence can occur from covariance within a network’s decision boundaries. See the top panel of Figure 1(b) for a simulated depiction of harmless divergence caused by covariance along causal dimensions. We see diverging intervened representations created by swapping the first causal dimension of sampled natural latents. However, the divergence remains within the desired decision boundaries, resulting in the appropriate counterfactual behavior.

We expand this intuition using a *behaviorally binary subspace* as an example, where we define a behaviorally binary subspace as one in which causally impacts the outputs of the next processing layer (e.g., classification labels) only through its sign. Formally, let $f : \mathbb{R}^d \rightarrow \mathbb{R}^k$ denote the next processing layer where k is the output dimensionality. Let $\text{sign}(\cdot)$ denote the elementwise sign map $\text{sign} : \mathbb{R}^{d_{\text{var}}} \rightarrow \{-1, 0, 1\}^{d_{\text{var}}}$, and assume a fixed alignment function \mathcal{A} and subspace selection matrix $D_{\text{var}} \in \mathbb{R}^{d \times d}$. A linear subspace $Z \subseteq \mathbb{R}^d$ is *behaviorally binary* (with respect to f , D_{var} , and \mathcal{A}) iff for all $D_{\text{var}}\mathcal{A}(h), D_{\text{var}}\mathcal{A}(h') \in Z$,

$$\text{sign}(D_{\text{var}}\mathcal{A}(h)) = \text{sign}(D_{\text{var}}\mathcal{A}(h')) \implies f(h) = f(h') \quad (4)$$

Now, suppose we have an NN with two causal subspaces, $\tilde{z}_{\text{var}_a} \subseteq \mathbb{R}^{d_{\text{var}_a}}$ and $\tilde{z}_{\text{var}_b} \subseteq \mathbb{R}^{d_{\text{var}_b}}$, with values $\tilde{z}_{\text{var}_a}^{(x_i)}$ and $\tilde{z}_{\text{var}_b}^{(x_i)}$, for a model input x_i , where we use the bold, tilde notation to distinguish variables from their values. Furthermore, assume that \tilde{z}_{var_b} is a behaviorally binary subspace that co-varies with, \tilde{z}_{var_a} . Using $h^{(x_i)}$ and $z^{(x_i)}$ from Equation 1 under a given input x_i , we use the following definition:

$$\mathcal{A}(h^{(x_i)}) = z^{(x_i)} = \begin{bmatrix} \tilde{z}_{\text{var}_a}^{(x_i)} = \tilde{z}_{\text{var}_a}^{(x_i)} \\ \tilde{z}_{\text{var}_b}^{(x_i)} = \tilde{z}_{\text{var}_b}^{(x_i)} \end{bmatrix} \quad (5)$$

Due to the assumption of covariance in $\tilde{\mathbf{z}}_{\text{var}_a}$ and $\tilde{\mathbf{z}}_{\text{var}_b}$, it is reasonable to assume that the values $\tilde{z}_{\text{var}_b}^{(x_{\text{low}})}$ and $\tilde{z}_{\text{var}_b}^{(x_{\text{high}})}$ are systematically distinct for distinct values of $\tilde{\mathbf{z}}_{\text{var}_a}$ under some classes of inputs, x_{low} and x_{high} , while $\text{sign}(\tilde{z}_{\text{var}_b}^{(x_{\text{low}})}) = \text{sign}(\tilde{z}_{\text{var}_b}^{(x_{\text{high}})})$. Under these assumptions, if we perform an interchange intervention on $\tilde{\mathbf{z}}_{\text{var}_b}$ using source representations from input x_{low} and target representations from input x_{high} , the intervened representation will have values:

$$\hat{z} = \begin{bmatrix} \tilde{\mathbf{z}}_{\text{var}_a} = \tilde{z}_{\text{var}_a}^{(x_{\text{high}})} \\ \tilde{\mathbf{z}}_{\text{var}_b} = \tilde{z}_{\text{var}_b}^{(x_{\text{low}})} \end{bmatrix} \quad (6)$$

Because we assumed that the value of $\tilde{z}_{\text{var}_b}^{(x_{\text{low}})}$ is systematically unique due to covariance in $\tilde{\mathbf{z}}_{\text{var}_a}$ and $\tilde{\mathbf{z}}_{\text{var}_b}$, the values $\tilde{z}_{\text{var}_a}^{(x_{\text{high}})}$ and $\tilde{z}_{\text{var}_b}^{(x_{\text{low}})}$ in Equation 6 will have never existed together in the native distribution, but the behavior of the NN will remain unchanged because $\tilde{\mathbf{z}}_{\text{var}_b}$ is behaviorally binary and its sign has not changed. This is thus a case of harmless divergence.

If we focus only on the divergence in causal subspaces and ignore cases of null-space interactions, what claims can we make about the model's natural neural mechanisms using divergent, intervened representations? An interpretation consistent with the principles of superposition (Smolensky, 1988; Rumelhart et al., 1986; McClelland et al., 1986; Elhage et al., 2022) is that differences in the exact values of each causal subspace do not matter – rather, *only the decision boundaries* along these subspaces matter. Under this interpretation, any divergence in the intervened distribution arising from covariance in causal subspaces is okay, because the separation of the causal subspaces and their decision boundaries—the computationally important aspects of the NN—are respected in the alignment. This interpretation allows us to ignore computationally irrelevant covariance in our attempt to understand NN mechanisms.

4.2 PERNICIOUS DIVERGENCE VIA OFF-MANIFOLD ACTIVATION

We call a *hidden pathway* any unit, vector direction, or subcircuit that is inactive on the natural support of representations but becomes active and influences behavior under an intervention. Hidden pathways are compatible with benign divergences (Sec. 4.1), yet they undermine claims about native mechanisms, and they can prime *dormant behavioral changes* (Sec. 4.2.2).

Formally, let \mathcal{D} denote the data distribution over latent representations $h^\ell \in \mathbb{R}^d$ at layer ℓ , and let $\mathcal{S} = \text{supp}(h^\ell \sim \mathcal{D})$ denote its support. Denoting the intended class K following an intervention as subscripted $\rightarrow K$, an intervened representation $\hat{h}_{\rightarrow K}^\ell$ is said to be *divergent* if $\hat{h}_{\rightarrow K}^\ell \notin \mathcal{S}$ or if it causes a ReLU state change for any neuron that does not change sign for the same class K under \mathcal{S} . We define the convex hull of class- K representations as $\text{conv}(S_K) = \{\sum_i \alpha_i h_{i,K}^\ell : \alpha_i \geq 0, \sum_i \alpha_i = 1\}$ where the subscript K denotes that $h_{i,K}^\ell$ was taken from class K inputs. Projecting an intervention onto $\text{conv}(S_K)$ ensures that it remains within the convex interpolation region of class- K samples.

4.2.1 MEAN-DIFFERENCE PATCHING ACTIVATES HIDDEN PATHWAYS

Claim. Patching with a mean-difference vector can flip a decision by activating a unit that is silent for all natural class inputs.

Setup. Consider a two-layer circuit with a ReLU nonlinearity. Let $h^\ell \in \mathbb{R}^4$ feed into

$$s = \mathbf{1}^\top h^{\ell+1} = \mathbf{1}^\top \text{ReLU}(W_\ell h^\ell + b_\ell), \quad W_\ell \in \mathbb{R}^{3 \times 4}, b_\ell \in \mathbb{R}^3,$$

where

$$W_\ell = \begin{bmatrix} 0.75 & 0.25 & 0 & 0.5 \\ 0 & 1 & 0 & 0 \\ 1 & 1 & -1 & -1 \end{bmatrix}, \quad b_\ell = \begin{bmatrix} -0.5 \\ -0.5 \\ 0 \end{bmatrix}.$$

A positive score ($s > 0$) indicates class A. Suppose class-A and class-B representations at layer ℓ are

$$h_A^\ell = \begin{cases} [1, 0, 1, 0]^\top & (\text{case 1}) \\ [0, 1, 1, 0]^\top & (\text{case 2}) \end{cases}, \quad h_B^\ell = \begin{cases} [0, 0, 1, 0]^\top & (\text{case 1}) \\ [0, 0, 1, 1]^\top & (\text{case 2}) \end{cases}$$

Evaluating h_A^ℓ yields

$$h_{A_{\text{case}_1}}^{\ell+1} = [0.25, 0, 0]^\top, \quad h_{A_{\text{case}_2}}^{\ell+1} = [0, 0.5, 0]^\top,$$

so $s_A \in \{0.25, 0.5\}$. For class B, all outputs are zero, $s_B = 0$.

Mean-difference patching. We construct a mean difference vector between the classes,

$$\delta_{B \rightarrow A} = \mu_A - \mu_B = \frac{1}{2} \sum_{i=1}^2 (h_{A_{\text{case}_i}}^\ell) - \frac{1}{2} \sum_{i=1}^2 (h_{B_{\text{case}_i}}^\ell) = [0.5, 0.5, 0, -0.5]^\top.$$

Applying this to class B representations gives

$$\hat{h}_{B \rightarrow A}^\ell = h_B^\ell + \delta_{B \rightarrow A} = \begin{cases} [0.5, 0.5, 1, -0.5]^\top & (\text{case 1}) \\ [0.5, 0.5, 1, 0.5]^\top & (\text{case 2}) \end{cases}$$

After propagation through the circuit:

$$\hat{h}_{B \rightarrow A}^{\ell+1} = \begin{cases} [0, 0, 0.5]^\top, & \hat{s}_{\text{case}_1} = 0.5 \\ [0.25, 0, 0]^\top, & \hat{s}_{\text{case}_2} = 0.25 \end{cases}$$

The intervention flips the decision to class A ($\hat{s} > 0$). However, the third hidden unit becomes active only for $\hat{h}_{B \rightarrow A}^\ell$, never for natural h_A^ℓ . This new activation is a *hidden pathway* that was silent under all native samples. Thus the mean-difference patch crosses the decision boundary only by activating an off-manifold circuit.

If we project $\hat{h}_{B \rightarrow A}^\ell$ onto $\text{conv}(S_A)$ (or equivalently onto a local PCA subspace of S_A), this ReLU state change disappears, and the decision boundary is no longer crossed—confirming that the original effect was driven by an off-manifold activation rather than a genuine within-manifold causal mechanism.

General condition. Let u_k^\top denote row k of W . If $u_k^\top h + b_k \leq 0$ for all $h \in S_A$ but $u_k^\top (h_B + \delta_{B \rightarrow A}) + b_k > 0$ for some h_B , then $\delta_{B \rightarrow A}$ activates a hidden pathway.

4.2.2 DORMANT BEHAVIORAL CHANGES

Divergent representations can also yield *dormant behavioral changes*—interventions that appear behaviorally neutral in one context but alter predictions in another. This occurs when an off-manifold activation primes a downstream computation that only manifests under specific contextual inputs.

Illustration. Extend the network from the previous Section 4.2.1 by adding one row of zeros to W_ℓ and b_ℓ , producing $h^{\ell+1} \in \mathbb{R}^4$ where the final coordinate is always zero. Add a context vector $v \in \mathbb{R}^4$ and a final affine layer:

$$\hat{y} = W_{\ell+1}(h^{\ell+1} + v) + b_{\ell+1}, \quad W_{\ell+1} = \begin{bmatrix} 1 & 1 & 0.5 & 0 \\ 0 & 0 & 0 & 0 \\ 0 & 0 & 1 & 1 \end{bmatrix}, \quad b_{\ell+1} = \begin{bmatrix} 0 \\ 0.25 \\ -1 \end{bmatrix}.$$

Here, the argmax index of $\hat{y} = [\hat{y}_1, \hat{y}_2, \hat{y}_3]^\top$ corresponds to class predictions A, B, and C.

Assume $v = [0, 0, 0, v_4]^\top$. For $\hat{h}_{B_{\text{case}_1} \rightarrow A}^{\ell+1} = [0, 0, 0.5, 0]^\top$,

$$\hat{y}_1 = 0.25, \quad \hat{y}_2 = 0.25 \quad \hat{y}_3 = (0.5 + v_4) - 1 = v_4 - 0.5.$$

The model predicts class A when $v_4 < 0.75$ but switches to class C when $v_4 > 0.75$. Notably, v_4 would not naturally cause a class C prediction below a value of 1 due to the bias threshold. Thus the same intervention that was benign in one context ($v_4 < 0.75$) produces a behavioral flip in another ($1 > v_4 > 0.75$) purely due to the latent divergence priming a new pathway.

Implications. Dormant behavioral changes highlight that behaviorally “safe” interventions can still introduce hidden context dependencies. Detecting them would require evaluating across all possible contexts, which is infeasible in practice. Therefore, interventions should (1) report any newly active units relative to native ReLU patterns, (2) project perturbed representations onto local manifolds, and (3) test for context-sensitive output flips across nuisance dimensions.

Summary. Hidden pathways arise when off-manifold interventions activate neurons that never fire for native representations. Such pathways can alter causal conclusions even when behavior appears unchanged. Manifold-preserving projections and ReLU-pattern audits provide practical safeguards against these pernicious forms of divergence.

5 HOW MIGHT WE AVOID DIVERGENT REPRESENTATIONS?

We have thus far demonstrated that divergent representations are empirically common and that they can theoretically be harmless or pernicious depending on the functional landscape of the target model and the causal claims. In this section, we consider the question of how such divergences might be avoided. There are existing methods that constrain counterfactual features (in our case, intervened representations) directly to the natural manifold (Verma et al., 2024). However, we seek a method that generates principled interventions on intermediate representations that are constrained to be innocuous. In pursuit of this method, we modify and apply the Counterfactual Latent (CL) loss introduced in Grant (2025). We apply this in synthetic settings as a demonstration of how to reduce pernicious divergence by minimizing all divergence along causally relevant dimensions.

5.1 SYNTHETIC MODEL SETTING

We simulate an intermediate layer of an NN by constructing a synthetic dataset of h vectors with known feature dimensions and labels y that we use to train a Multi-Layer Perceptron (MLP). The dataset consists of noisy samples around a set of grid points from two feature dimensions with correlational structure. Specifically, we define a base set of points given by the Cartesian product of two values along the x_1 -axis, $\{-1, 1\}$, and five evenly spaced values along the x_2 -axis, $\{0, 1, 2, 3, 4\}$, resulting in ten unique base coordinates, each corresponding to 1 of 10 classes. We add noise and covariance to these feature dimensions and concatenate n extra noise dimensions resulting in simulated vectors $h \in \mathbb{R}^{2+n}$, where $n = 64$ unless otherwise stated. The feature dimensions of these synthetic vectors are shown as the natural distributions in Figures 1(b) and 3. We then train a small MLP on these representations to predict the class labels using a standard cross entropy loss. After training, we perform DAS with varying intensities of the behavioral and CL loss term. See Appendix A.2 for further details on the dataset construction, MLP training, and DAS trainings.

5.2 ADAPTED COUNTERFACTUAL LATENT LOSS

To encourage intervened representations to be more similar to the native distribution of NN representations, we build upon the CL auxiliary loss from Grant (2025). This auxiliary objective relies on *counterfactual latent (CL) vectors* as vector objectives. CL vectors are defined as vectors that encode the same causal variable value(s) that *would* exist in the intervened vector, \hat{h} , assuming the interchange intervention was successful. We can obtain CL vectors by searching through a pre-recorded set of natural h vectors for situations and behaviors that are consistent with the values of the causal abstraction to which we are aligning. See Figure 3(a) for a visualization. As an example, assume that we have a CA with variables var_u , var_w , and $\text{var}_{\text{extra}}$, and following a causal intervention we expect \hat{h} to have a value of u for variable var_u and w for variable var_w . The CL vector h_{CL} in this example can be obtained from averaging over a set of m natural representations, $h_{\text{CL}} = \frac{1}{m} \sum_{i=1}^m h_{\text{CL}}^{(x_i)}$, where each $h_{\text{CL}}^{(x_i)}$ has the same variable values: $\text{var}_u = u$ and $\text{var}_w = w$ labeled by the CA. Note that Grant (2025) constructed h_{CL} using $m = 1$, whereas we use m equal to all valid $h_{\text{CL}}^{(x_i)}$ in the dataset.

The CL auxiliary loss \mathcal{L}_{CL} introduced in Grant (2025) is composed of the mean of an L2 and a cosine distance minimization objective using CL vectors as labels. In this work, we modify this loss by applying it to individual causal subspaces. This allows us to construct $h_{\text{CL}}^{\text{var}_i}$ vectors specific to a single causal variable var_i . Using notation defined in Section 2.2, the \mathcal{L}_{CL} for a single training sample is defined as follows:

$$\hat{z}^{\text{var}_i} = D_{\text{var}_i} \mathcal{A}(\hat{h}) \quad (7)$$

$$z_{\text{CL}}^{\text{var}_i} = D_{\text{var}_i} \mathcal{A}(h_{\text{CL}}) \quad (8)$$

$$\mathcal{L}_{\text{CL}} = \sum_{i=1}^n \mathcal{L}_{\text{CL}}^{\text{var}_i} = \sum_{i=1}^n \left(\frac{1}{2} \|\hat{z}^{\text{var}_i} - z_{\text{CL}}^{\text{var}_i}\|_2^2 - \frac{1}{2} \frac{\hat{z}^{\text{var}_i} \cdot z_{\text{CL}}^{\text{var}_i}}{\|\hat{z}^{\text{var}_i}\|_2 \|z_{\text{CL}}^{\text{var}_i}\|_2} \right) \quad (9)$$

The CL loss is combined with the DAS loss into a single loss term using ϵ as a tunable hyperparameter: $\mathcal{L}_{\text{total}} = \epsilon \mathcal{L}_{\text{CL}} + \mathcal{L}_{\text{DAS}}$. The loss is computed as the mean over batches of samples and optimized using gradient descent (Appendix A.2).

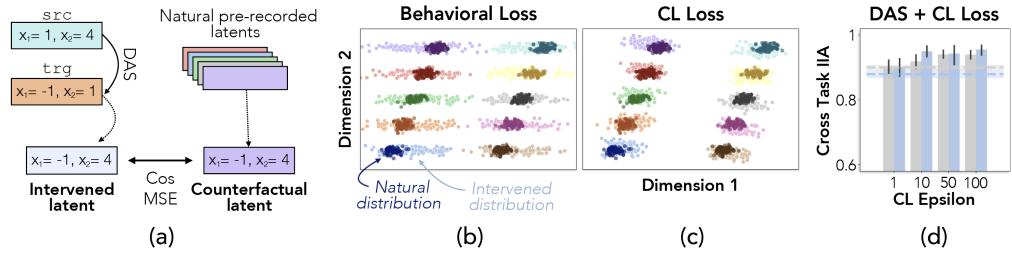


Figure 3: **The CL loss reduces representational divergence and improves out-of-distribution generalization.** (a) Diagram of the CL loss. The rectangles represent model latent vectors. x_1 and x_2 indicate the latent state’s non-noisy values of the two synthetic, causal dimensions shown in panels (b) and (c), labeled by the causal abstraction. We patch the x_2 value from the source vector into the target using DAS. The modified counterfactual latent (CL) loss vector is defined as the average over all naturally occurring latent vectors that possess the same variable values as the post-intervention latent vector. (b) Each panel shows the two causal feature dimensions of hidden states (represented by each dot) from a synthetic dataset. Colors indicate the class of the hidden state; dark dots indicate that the state is from the natural distribution while lighter dots indicate that the state is from the intervened distribution. The leftmost panel shows results from DAS trained using behavior only (Equation 3), the rightmost panel shows DAS trained on only the CL loss (Equation 9). We can see that the CL loss reduces the divergence along the feature dimensions.

5.3 THE CL LOSS ALLEVIATES DIVERGENCE AND CAN IMPROVE GENERALIZATION

Figures 3(b) and 3(c) provide a qualitative comparison of intervened and native representations for interventions using a trained DAS rotation matrix. Each dot in the figures shows the values of the feature dimensions for a single representation. The native states are displayed in darker colors and the intervened in lighter. Each hue indicates the ground truth class of the state. We can see a tightening of the intervened representations with increasing intensity of the CL loss. Quantitatively, the DAS loss produces EMD values along the feature dimensions of 0.043 ± 0.002 whereas the CL loss produces 0.024 ± 0.001 with IIA values of 0.981 ± 0.003 and 0.977 ± 0.004 respectively.

We hypothesized that reduced divergence could improve IIA when transferring the DAS rotation matrix to OOD settings. To test this, we partitioned the synthetic task into a Dense and a Sparse group, named for the relative spacing of 4 distinct classes within each group. See Appendix A.2.4 for further details on the partitions. We then performed DAS on each of the partitions and evaluated the performance on the held-out partition to produce the results in Figure 3(d). The CL loss performs better than the behavioral loss in these OOD settings. We provide further exploration of the CL loss IIA and EMD across a range of hyperparameters in Appendix A.2.5.

6 DISCUSSION AND LIMITATIONS

In this work we demonstrated that a variety of common causal interventions can produce representations that diverge from a target model’s original distribution of latent representations. We then showed that although such divergences can have benign effects for many causal claims, they can also activate hidden pathways and trigger dormant behaviors that can perniciously affect other claims. As a step towards mitigating this issue, we provided a broad-stroke solution by directly minimizing the divergence of intervened activity along causal dimensions, mitigating both pernicious and harmless forms of divergence.

A remaining gap in our work is the failure to produce a reliable method for classifying pernicious forms of divergent representations. Additionally, the CL loss that we have presented is confined to a narrow set of simplistic settings and is not specific to pernicious divergence. We look forward to exploring ways to classify and mitigate pernicious divergence through self-supervised means in future work.

Where does this leave us with respect to causal interventions in mechanistic interpretability? Given our theoretical findings, any divergence outside of the null-space of NN layers is potentially pernicious.

This poses challenges for aspirations of a complete mechanistic understanding of NNs using existing methods alone. However, we note that many practical mechanistic projects can be satisfied by collecting sufficiently large intervention evaluation datasets, and continued development of methods such as the CL loss can reduce the problem even further. We are optimistic for future developments in this field.

7 ACKNOWLEDGMENTS

Thank you to the PDP Lab and the Stanford Psychology department for funding. Thank you to Noah Goodman and Jay McClelland for thoughtful feedback and discussions. Thank you to the PDP lab and the Stanford Mech Interp community for opportunities to present and for thoughtful discussion.

REFERENCES

Joseph Bloom, Curt Tigges, Anthony Duong, and David Chanin. Saelens. <https://github.com/jbloomAus/SAELens>, 2024.

Lukas Braun, Erin Grant, and Andrew M Saxe. Not all solutions are created equal: An analytical dissociation of functional and representational similarity in deep linear neural networks. In *Forty-second International Conference on Machine Learning*, 2025. URL <https://openreview.net/forum?id=YucuAuXMpT>.

Hang Chen, Jiaying Zhu, Xinyu Yang, and Wenya Wang. Rethinking circuit completeness in language models: And, or, and adder gates. *arXiv preprint arXiv:2505.10039*, 2025.

Róbert Csordás, Christopher Potts, Christopher D. Manning, and Atticus Geiger. Recurrent neural networks learn to store and generate sequences using non-linear representations, 2024. URL <https://arxiv.org/abs/2408.10920>.

Marco Cuturi. Sinkhorn distances: Lightspeed computation of optimal transport. In *Advances in Neural Information Processing Systems*, pp. 2292–2300, 2013.

Qin Dai, Benjamin Heinzerling, and Kentaro Inui. Representational analysis of binding in language models. *arXiv preprint arXiv:2409.05448*, 2024.

Nelson Elhage, Tristan Hume, Catherine Olsson, Nicholas Schiefer, Tom Henighan, Shauna Kravec, Zac Hatfield-Dodds, Robert Lasenby, Dawn Drain, Carol Chen, Roger Grosse, Sam McCandlish, Jared Kaplan, Dario Amodei, Martin Wattenberg, and Christopher Olah. Toy models of superposition. *Transformer Circuits Thread*, 2022. https://transformer-circuits.pub/2022/toy_model/index.html.

Jiahai Feng and Jacob Steinhardt. How do language models bind entities in context?, 2024. URL <https://arxiv.org/abs/2310.17191>.

Atticus Geiger, Kyle Richardson, and Christopher Potts. Neural natural language inference models partially embed theories of lexical entailment and negation. *arXiv preprint arXiv:2004.14623*, 2020.

Atticus Geiger, Hanson Lu, Thomas Icard, and Christopher Potts. Causal abstractions of neural networks. *CoRR*, abs/2106.02997, 2021. URL <https://arxiv.org/abs/2106.02997>.

Atticus Geiger, Zhengxuan Wu, Christopher Potts, Thomas Icard, and Noah D. Goodman. Finding alignments between interpretable causal variables and distributed neural representations, 2023.

Atticus Geiger, Duligur Ibeling, Amir Zur, Maheep Chaudhary, Sonakshi Chauhan, Jing Huang, Aryaman Arora, Zhengxuan Wu, Noah Goodman, Christopher Potts, and Thomas Icard. Causal abstraction: A theoretical foundation for mechanistic interpretability, 2024. URL <https://arxiv.org/abs/2301.04709>.

Atticus Geiger, Jacqueline Harding, and Thomas Icard. How causal abstraction underpins computational explanation. *arXiv preprint arXiv:2508.11214*, 2025.

Satchel Grant. Model alignment search. *arXiv preprint arXiv:2501.06164*, 2025.

Satchel Grant, Noah D. Goodman, and James L. McClelland. Emergent symbol-like number variables in artificial neural networks. *Transactions on Machine Learning Research*, 2024. URL <https://arxiv.org/abs/2501.06141>.

Stefan Heimersheim and Neel Nanda. How to use and interpret activation patching. *arXiv preprint arXiv:2404.15255*, 2024.

Jing Huang, Zhengxuan Wu, Christopher Potts, Mor Geva, and Atticus Geiger. RAVEL: Evaluating interpretability methods on disentangling language model representations. In Lun-Wei Ku, Andre Martins, and Vivek Srikumar (eds.), *Proceedings of the 62nd Annual Meeting of the Association for Computational Linguistics (Volume 1: Long Papers)*, pp. 8669–8687, Bangkok, Thailand, August 2024. Association for Computational Linguistics. URL <https://aclanthology.org/2024.acl-long.470>.

Sergey Ioffe and Christian Szegedy. Batch normalization: Accelerating deep network training by reducing internal covariate shift. In *International conference on machine learning*, pp. 448–456. pmlr, 2015.

Diederik P. Kingma and Jimmy Ba. Adam: A method for stochastic optimization, 2017.

Andrew Kyle Lampinen, Stephanie CY Chan, Yuxuan Li, and Katherine Hermann. Representation biases: will we achieve complete understanding by analyzing representations? *arXiv preprint arXiv:2507.22216*, 2025.

LawrenceC, Adrià Garriga-alonso, Nicholas Goldowsky-Dill, ryan_greenblatt, jenny, Ansh Radhakrishnan, Buck, and Nate Thomas. Causal Scrubbing: a method for rigorously testing interpretability hypotheses [Redwood Research]. *Less Wrong*, dec 2022. URL <https://www.alignmentforum.org/posts/JvZhzyCHu2Yd57RN/causal-scrubbing-a-method-for-rigorously-testing>.

Jack Lindsey, Wes Gurnee, Emmanuel Ameisen, Brian Chen, Adam Pearce, Nicholas L. Turner, Craig Citro, David Abrahams, Shan Carter, Basil Hosmer, Jonathan Marcus, Michael Sklar, Adly Templeton, Trenton Bricken, Callum McDougall, Hoagy Cunningham, Thomas Henighan, Adam Jermyn, Andy Jones, Andrew Persic, Zhenyi Qi, T. Ben Thompson, Sam Zimmerman, Kelley Rivoire, Thomas Conerly, Chris Olah, and Joshua Batson. On the biology of a large language model. *Transformer Circuits Thread*, 2025. URL <https://transformer-circuits.pub/2025/attribution-graphs/biology.html>.

Aleksandar Makelov, Georg Lange, and Neel Nanda. Is this the subspace you are looking for? an interpretability illusion for subspace activation patching. *arXiv preprint arXiv:2311.17030*, 2023.

J. L. McClelland, D. E. Rumelhart, and PDP Research Group (eds.). *Parallel Distributed Processing. Volume 2: Psychological and Biological Models*. MIT Press, Cambridge, MA, 1986.

Kevin Meng, David Bau, Alex Andonian, and Yonatan Belinkov. Locating and editing factual associations in gpt, 2023. URL <https://arxiv.org/abs/2202.05262>.

Maxime Méloux, Silviu Maniu, François Portet, and Maxime Peyrard. Everything, Everywhere, All at Once: Is Mechanistic Interpretability Identifiable? In *Workshop on Mechanistic Interpretability*, oct 2024. URL <https://openreview.net/forum?id=5IWJBStfU7>.

Neel Nanda. Attribution patching: Activation patching at industrial scale. <https://www.neelnanda.io/mechanistic-interpretability/attribution-patching>, 2022.

Judea Pearl. An Introduction to Causal Inference. *The International Journal of Biostatistics*, 6(2):7, February 2010. ISSN 1557-4679. doi: 10.2202/1557-4679.1203. URL <https://www.ncbi.nlm.nih.gov/pmc/articles/PMC2836213/>.

D. E. Rumelhart, J. L. McClelland, and PDP Research Group (eds.). *Parallel Distributed Processing. Volume 1: Foundations*. MIT Press, Cambridge, MA, 1986.

Claudia Shi, Nicolas Beltran Velez, Achille Nazaret, Carolina Zheng, Adrià Garriga-Alonso, Andrew Jesson, Maggie Makar, and David Blei. Hypothesis testing the circuit hypothesis in llms. *Advances in Neural Information Processing Systems*, 37:94539–94567, 2024.

Paul Smolensky. On the proper treatment of connectionism. *Behavioral and Brain Sciences*, 11(1):1–23, 1988. doi: 10.1017/S0140525X00052432.

Nitish Srivastava, Geoffrey Hinton, Alex Krizhevsky, Ilya Sutskever, and Ruslan Salakhutdinov. Dropout: A simple way to prevent neural networks from overfitting. *Journal of Machine Learning Research*, 15(56):1929–1958, 2014. URL <http://jmlr.org/papers/v15/srivastava14a.html>.

David Stutz, Matthias Hein, and Bernt Schiele. Disentangling adversarial robustness and generalization. In *Proceedings of the IEEE/CVF conference on computer vision and pattern recognition*, pp. 6976–6987, 2019.

Denis Sutter, Julian Minder, Thomas Hofmann, and Tiago Pimentel. The non-linear representation dilemma: Is causal abstraction enough for mechanistic interpretability? *arXiv preprint arXiv:2405.05847*, 2025. URL <https://arxiv.org/abs/2507.08802>.

Hugo Touvron, Thibaut Lavril, Gautier Izacard, Xavier Martinet, Marie-Anne Lachaux, Timothée Lacroix, Baptiste Rozière, Naman Goyal, Eric Hambro, Faisal Azhar, Aurelien Rodriguez, Armand Joulin, Edouard Grave, and Guillaume Lample. Llama: Open and efficient foundation language models, 2023.

Asterios Tsiorvas, Wei Sun, and Georgia Perakis. Manifold-aligned counterfactual explanations for neural networks. In Sanjoy Dasgupta, Stephan Mandt, and Yingzhen Li (eds.), *Proceedings of The 27th International Conference on Artificial Intelligence and Statistics*, volume 238 of *Proceedings of Machine Learning Research*, pp. 3763–3771. PMLR, 02–04 May 2024. URL <https://proceedings.mlr.press/v238/tsiorvas24a.html>.

Sahil Verma, Varich Boonsanong, Minh Hoang, Keegan Hines, John Dickerson, and Chirag Shah. Counterfactual explanations and algorithmic recourses for machine learning: A review. *ACM Comput. Surv.*, 56(12), October 2024. ISSN 0360-0300. doi: 10.1145/3677119. URL <https://doi.org/10.1145/3677119>.

Jesse Vig, Sebastian Gehrmann, Yonatan Belinkov, Sharon Qian, Daniel Nevo, Simas Sakenis, Jason Huang, Yaron Singer, and Stuart Shieber. Causal mediation analysis for interpreting neural nlp: The case of gender bias. *arXiv preprint arXiv:2004.12265*, 2020.

Cédric Villani. The wasserstein distances. In *Optimal Transport: Old and New*, pp. 94–105. Springer, Berlin, Heidelberg, 2009. doi: 10.1007/978-3-540-71050-9_6.

Kevin Wang, Alexandre Variengien, Arthur Conmy, Buck Shlegeris, and Jacob Steinhardt. Interpretability in the wild: a circuit for indirect object identification in gpt-2 small, 2022. URL <https://arxiv.org/abs/2211.00593>.

Martin Wattenberg and Fernanda B. Viégas. Relational Composition in Neural Networks: A Survey and Call to Action, July 2024. URL <http://arxiv.org/abs/2407.14662>. arXiv:2407.14662 [cs].

Thomas Wolf, Lysandre Debut, Victor Sanh, Julien Chaumond, Clement Delangue, Anthony Moi, Pierrick Cistac, Timothée Rault, Rémi Louf, Morgan Funtowicz, Jamie Davison, Sam Shleifer, Patrick von Platen, Qi Ma, Mariama Jernite, Julien Plu, Liwen Xu, Teven Lhoest, Giancarlo Maggiore, Pietro Paul, Umar Ruwase, Jacob Devlin, Matt Tomei, Margaret U Gorman, Eric Jurgens, and Alexander M Rush. HuggingFace’s Transformers: State-of-the-art Natural Language Processing. *arXiv preprint arXiv:1910.03771*, 2019.

Zhengxuan Wu, Atticus Geiger, Thomas Icard, Christopher Potts, and Noah Goodman. Interpretability at scale: Identifying causal mechanisms in alpaca. *Advances in neural information processing systems*, 36:78205–78226, 2023.

Fred Zhang and Neel Nanda. Towards Best Practices of Activation Patching in Language Models: Metrics and Methods, January 2024. URL <http://arxiv.org/abs/2309.16042>. arXiv:2309.16042 [cs] version: 2.

A APPENDIX

A.1 EMPIRICAL INTERVENED DIVERGENCE METHODOLOGICAL DETAILS

A.1.1 INTERVENTION METHODS

We considered three families of interpretability interventions that modify hidden-layer representations. In all three, we visualize the residual stream output from the specified layer:

1. **Mean Difference Vector Patching (MDVP)** (Feng & Steinhardt, 2024), where an intervention vector $\delta_{\text{MD}} \in \mathbb{R}^d$ is defined as the difference in mean activations between two conditions and then added to or subtracted from activations $h \in \mathbb{R}^d$. Formally,

$$\hat{h} = h + \delta_{\text{MD}} \quad (10)$$

We examine the representations \hat{h} from a sample size of 100 unique contexts across 4 token positions at each individual layer. We compare the representations to the native cases of the swapped binding positions. We used layer 10 of Meta’s Meta-Llama-3-8B-Instruct through Huggingface’s transformers package for this task and visualization (Touvron et al., 2023; Wolf et al., 2019). We selected layer 10 as it had the lowest EMD difference of all layers, although, we note that this measure did not necessarily correlate with the subjective interpretation of divergence in the qualitative visualizations. We report the EMD difference in Figure 2(a) as the average over all model layers.

2. **Sparse Autoencoder (SAE) Projections** (Bloom et al., 2024), where h is projected through a trained encoder $E : \mathbb{R}^d \rightarrow \mathbb{R}^k$ and linear decoder $D : \mathbb{R}^k \rightarrow \mathbb{R}^d$:

$$h' = D(E(h)). \quad (11)$$

SAEs are trained with sparsity penalty λ_{SAE} to encourage interpretable basis functions. We offload further experimental details to the referenced SAElens paper and code base. We compare the reconstructed representations to an equal sample size of 2000 vectors from the natural distribution. We used layer 25 of Meta’s Meta-Llama-3-8B-Instruct through Huggingface’s transformers package for this task and visualization (Touvron et al., 2023; Wolf et al., 2019). We selected layer 25 as it appeared to be the only layer available through SAElens’ pretrained SAEs.

3. **Distributed Alignment Search (DAS)** (Wu et al., 2023), where representations are aligned to a causal abstraction using a learned orthogonal transformation $Q \in \mathbb{R}^{d \times d}$. See Section 2.2 and Wu et al. (2023) for further detail on the method. We compare the intervened representations to an equal sample size of 1000 vectors from the natural distribution. We used the model and layer specified in Wu et al. (2023) for the visualizations in Figure 2.

A.1.2 MEASURING DIVERGENCE

To quantify distributional shifts between original and intervened representations, we approximated the **Earth Mover’s Distance (EMD)** (Villani, 2009) using the Sinkhorn loss from the GeomLoss python package with a $p = 2$ and blur = 0.05 (Cuturi, 2013). Let $\mathcal{H} = \{h_i\}_{i=1}^N$ denote a set of original representations and $\hat{\mathcal{H}} = \{\hat{h}_i\}_{i=1}^N$ their intervened counterparts. We computed

$$\text{EMD}(\mathcal{H}, \hat{\mathcal{H}}) = \min_{\gamma \in \Pi(\mu, \nu)} \sum_{i,j} \gamma_{ij} \|h_i - \hat{h}_j\|_2, \quad (12)$$

where μ and ν are the empirical distributions over \mathcal{H} and $\hat{\mathcal{H}}$, and $\Pi(\mu, \nu)$ denotes the set of couplings with marginals μ and ν .

Baseline correction. To isolate divergence due specifically to intervention, we subtracted a baseline EMD, computed by comparing the original set \mathcal{H} to a separately sampled set \mathcal{H}' :

$$\text{Divergence} = \text{EMD}(\mathcal{H}, \hat{\mathcal{H}}) - \text{EMD}(\mathcal{H}, \mathcal{H}'). \quad (13)$$

A.1.3 VISUALIZATION

We visualized both original and intervened representations by projecting onto the first two principal components of the covariance matrix of \mathcal{H} and $\hat{\mathcal{H}}$ combined:

$$\text{PCs} = \text{eigenvectors} \left(\text{Cov} \left(\begin{bmatrix} \mathcal{H} \\ \hat{\mathcal{H}} \end{bmatrix} \right) \right). \quad (14)$$

The top two principal components were used to plot representations in two dimensions, with colors distinguishing intervention method and condition (Figure 2).

A.1.4 ACTIVATION PATCHING IN BALANCED SUBSPACES

Here we include an additional example of pernicious activation patching that assumes the existence of *balanced subspaces*, defined as one or more behaviorally relevant subspaces that are canceled out by opposing weight values. Before continuing, we note that such subspaces are unlikely to exist in practical models due to the fact that they would only arise in cases where two rows of a weight matrix $W \in \mathbb{R}^{n \times m}$ are non-zero, scalar multiples of one another, assuming $h = Wx$. This example, however, could arise in cases where the input x is low rank and a subset of the columns of two rows in W are scalar multiples of one another.

Consider the case where there exists an NN layer that classifies inputs based on the mean intensity of dimensions 3 and 4 for a latent vector $h \in \mathbb{R}^4$, where the NN layers that produce h are denoted $f(x)$ with data inputs x sampled from the dataset, $x \sim \mathcal{D}$, and where the layer of interest has a synthetically constructed weight vector $w \in \mathbb{R}^4$ where $w^\top = [w_1 \ w_2 \ w_3 \ w_4] = [1 \ -1 \ \frac{1}{2} \ \frac{1}{2}]$. The layer is thus defined as follows:

$$y = w^\top f(x^{(i)}) = w^\top h^{(i)} = 1h_1^{(i)} - 1h_2^{(i)} + \frac{1}{2}h_3^{(i)} + \frac{1}{2}h_4^{(i)} \quad (15)$$

Here, i denotes the index of the data within the dataset. Further assume that some behavioral decision depends on the sign of y , that h_1 and h_2 together form balanced subspaces given w (meaning that for all $x^{(i)} \sim \mathcal{D}$, $w_1 h_1^{(i)} = -w_2 h_2^{(i)}$), and that they are non-dormant, meaning that for some pairs $(x^{(i)}, x^{(j)})$ where $i \neq j$, then $h_1^{(i)} \neq h_1^{(j)}$. Under these assumptions, the subspace spanned by $[1 \ 0 \ 0 \ 0]^\top$ and $[0 \ 1 \ 0 \ 0]^\top$ is not causally affecting the network's output under the natural distribution of h . However, if we intervene on h_1 or h_2 while leaving h_3 and h_4 unchanged, the intervened representation \hat{h} will diverge and potentially cross the decision boundary.

Concretely, if we set $h^{(i)} = [1 \ 1 \ 1 \ 1]^\top$ and $h^{(j)} = [3 \ 3 \ -1 \ -1]^\top$ and then perform an intervention on h_2 using $h^{(i)}$ as the target and $h^{(j)}$ as the source, we get: $\hat{h} = [1 \ 3 \ 1 \ 1]^\top$. This will result in a negative value of y , thus crossing its decision boundary using a non-native mechanism. This intervention could be used as experimentally affirming evidence for a mechanistic claim, when in reality we have not addressed the model's original mechanism.

A.2 CL LOSS CONTINUED

A.2.1 SYNTHETIC DATASET CONSTRUCTION

We constructed a synthetic dataset of intermediate-layer representations $h \in \mathbb{R}^{66}$ with known ground-truth labels $y \in \{1, \dots, 10\}$ and two causal feature dimensions, where 66 comes from 2 feature dimensions plus 64 concatenated noise dimensions is the total feature dimensionality.

Base feature coordinates. We first defined a grid of base coordinates as the Cartesian product of $\{-1, 1\}$ along the first feature axis and $\{0, 1, 2, 3, 4\}$ along the second feature axis:

$$\mathcal{G} = \{-1, 1\} \times \{0, 1, 2, 3, 4\}, \quad (16)$$

This procedure yields $10 = |\mathcal{G}|$ unique base coordinates, each corresponding to a distinct class label.

Noise and correlation structure. For each base coordinate $(x_1, x_2) \in \mathcal{G}$, we generated N noisy samples by adding Gaussian noise with variance 0.1^2 and covariance parameter 0.2. Specifically, each sample was drawn as

$$\begin{bmatrix} \tilde{x}_1 \\ \tilde{x}_2 \end{bmatrix} \sim \mathcal{N} \left(\begin{bmatrix} x_1 \\ x_2 \end{bmatrix}, \begin{bmatrix} 0.1^2 & 0.2 \\ 0.2 & 0.1^2 \end{bmatrix} \right). \quad (17)$$

Additional noise dimensions. We augmented each 2D noisy base vector with 64 independent Gaussian noise features, each sampled from $\mathcal{N}(0, 1)$, producing final representations $h \in \mathbb{R}^{2+64}$.

A.2.2 MLP TRAINING

We trained a feedforward Multi-Layer Perceptron (MLP) classifier to predict the class label y from the synthetic representations h . The MLP was parameterized with:

- input dimensionality d , defaulting to $d = 18$ as previously described
- a 1D batch normalization of d dimensions ([Ioffe & Szegedy, 2015](#)),
- one hidden layer of width 128,
- activation function ReLU,
- dropout with probability 0.5 to drop ([Srivastava et al., 2014](#)),
- a 1D batch normalization of 128 dimensions,
- output layer with 10 logits.

Training was performed with a standard categorical cross-entropy loss:

$$\mathcal{L}_{\text{CE}} = -\frac{1}{B} \sum_{i=1}^B \log p_{\theta}(y_i \mid h_i), \quad (18)$$

where B is the batch size and p_{θ} denotes the MLP’s predictive distribution over class labels. Optimization used stochastic gradient descent with learning rate 0.005 for 1000 epochs with early stopping using an Adam optimizer ([Kingma & Ba, 2017](#)). The code was implemented in PyTorch.

A.2.3 DAS TRAINING

Following MLP pretraining, we applied Distributed Alignment Search (DAS) with varying intensities of the behavioral loss and contrastive learning (CL) loss terms. Specifically, the DAS objective was

$$\mathcal{L}_{\text{DAS}} = \epsilon_{\text{behavior}} \mathcal{L}_{\text{behavior}} + \epsilon_{\text{CL}} \mathcal{L}_{\text{CL}}, \quad (19)$$

where $\epsilon_{\text{behavior}}$ and ϵ_{CL} are tunable coefficients controlling the strength of each term. We only use values of 0 or 1 for $\epsilon_{\text{behavior}}$ and we explore values of ϵ_{CL} referring to it as the CL epsilon in figures. We default to an overall learning rate of 0.05 and subspace size of 1 unless otherwise specified. Details of these loss functions are provided in Section 5.

A.2.4 OUT-OF-DISTRIBUTION EXPERIMENTAL DETAILS

To perform the OOD CL loss experiments, we partitioned the classes into 2 groups, excluding two classes from the partitions entirely. The groups were chosen so that the Sparse set had strictly greater spacing relative to the Dense set. See a visualization of the Dense and Sparse partitions in Figure 4(c). The trainings consisted of the described DAS training settings specified in Appendix A.2.3 except that the data during training was restricted to the respective data partitions. We show IIA values taken from the test sets of each partition.

A.2.5 FURTHER CL LOSS EXPLORATIONS

In these explorations, we explore DAS learning rate choices, number of mask dimensions, and the number of extra noisy dimensions for the OOD experiments. We show accuracies, EMD divergences, and EMD divergences restricted to the causal dimensions. The EMD values are scaled by the number of extra noisy dimensions concatenated to the input representations. We refer to the EMD measurements along causal dimensions only as the Row EMD. We do this for both the trained partitions and held-out partitions for various DAS trainings.

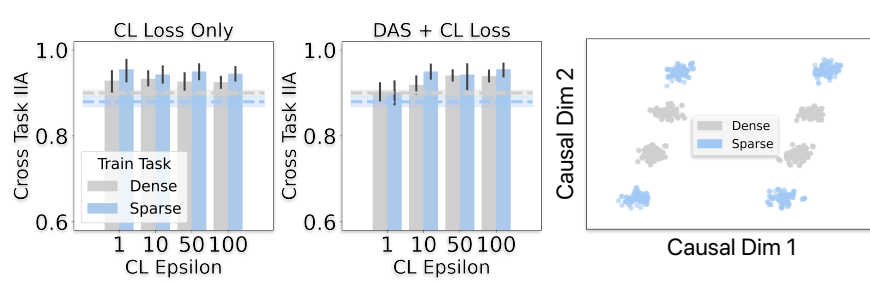


Figure 4: Out-of-distribution evaluation for DAS trained on the synthetic task with different loss variants. The dashed lines show results for DAS trained using only the behavioral loss. The grey hue indicates that DAS was trained to classify each of the four grey dots and evaluated on classifying the blue dots into their respective categories, and visa-versa for the blue hue. We see that in this setting, the CL loss provides performance benefits for out-of-distribution evaluation.

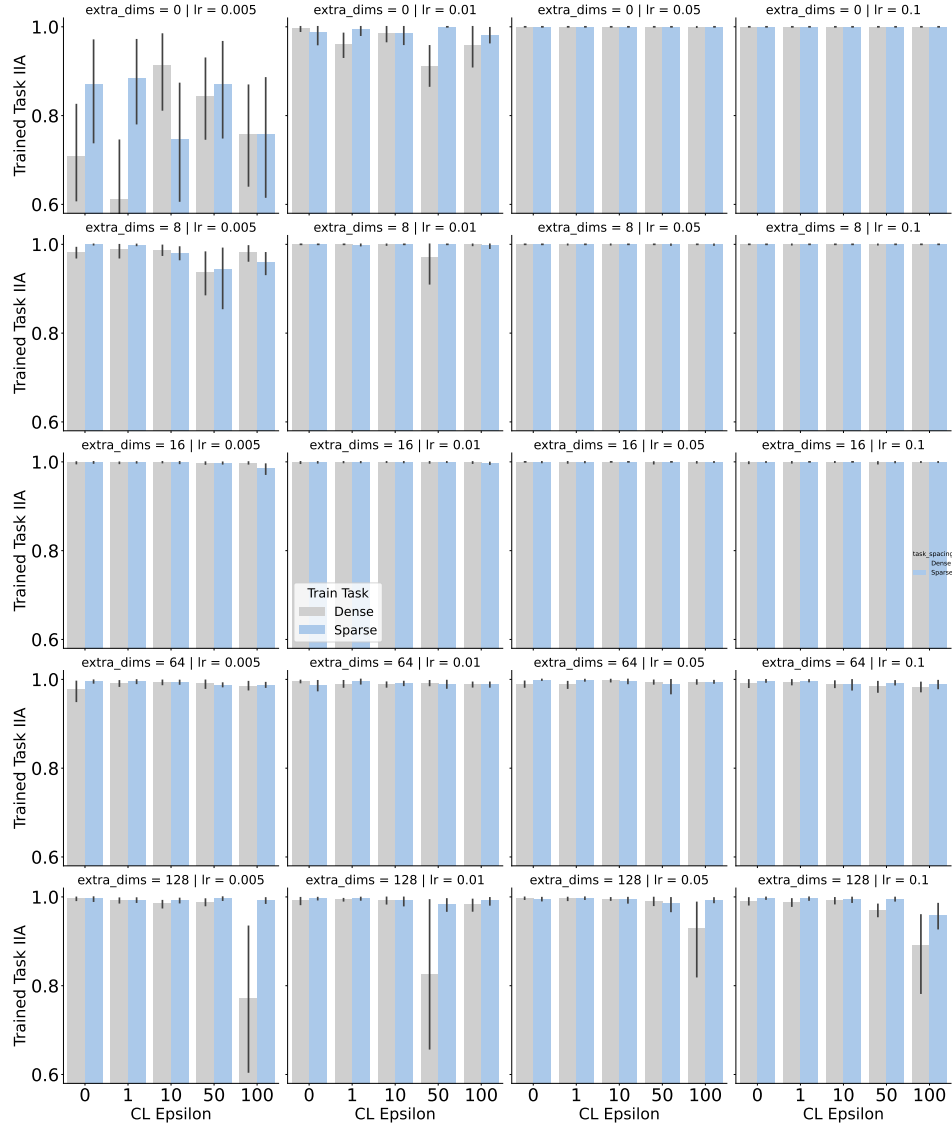


Figure 5: Within distribution hyperparameter search showing the DAS IIA on validation data for the trained task partition. We see the DAS loss learning rate (lr) and extra concatenated noisy input dimensions (extra_dim) across the panel columns and rows. All reported values include the behavioral loss with different values of the CL Epsilon (shown on the x-axis).

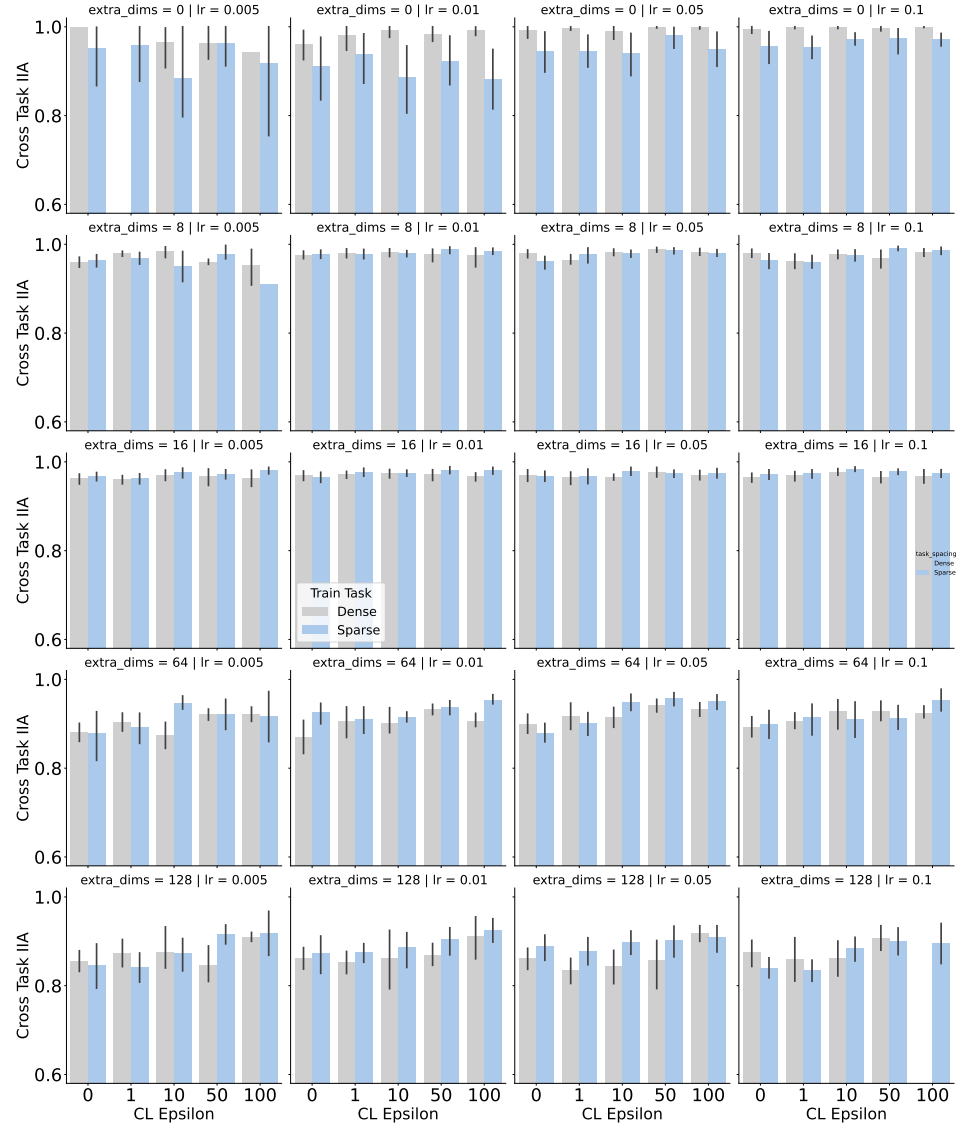


Figure 6: Out-of-distribution hyperparameter search showing the DAS IIA on validation data for the held-out task partition. We see the DAS loss learning rate (lr) and extra concatenated noisy input dimensions (extra_dim) across the panel columns and rows. All reported values include the behavioral loss with different values of the CL Epsilon (shown on the x-axis).

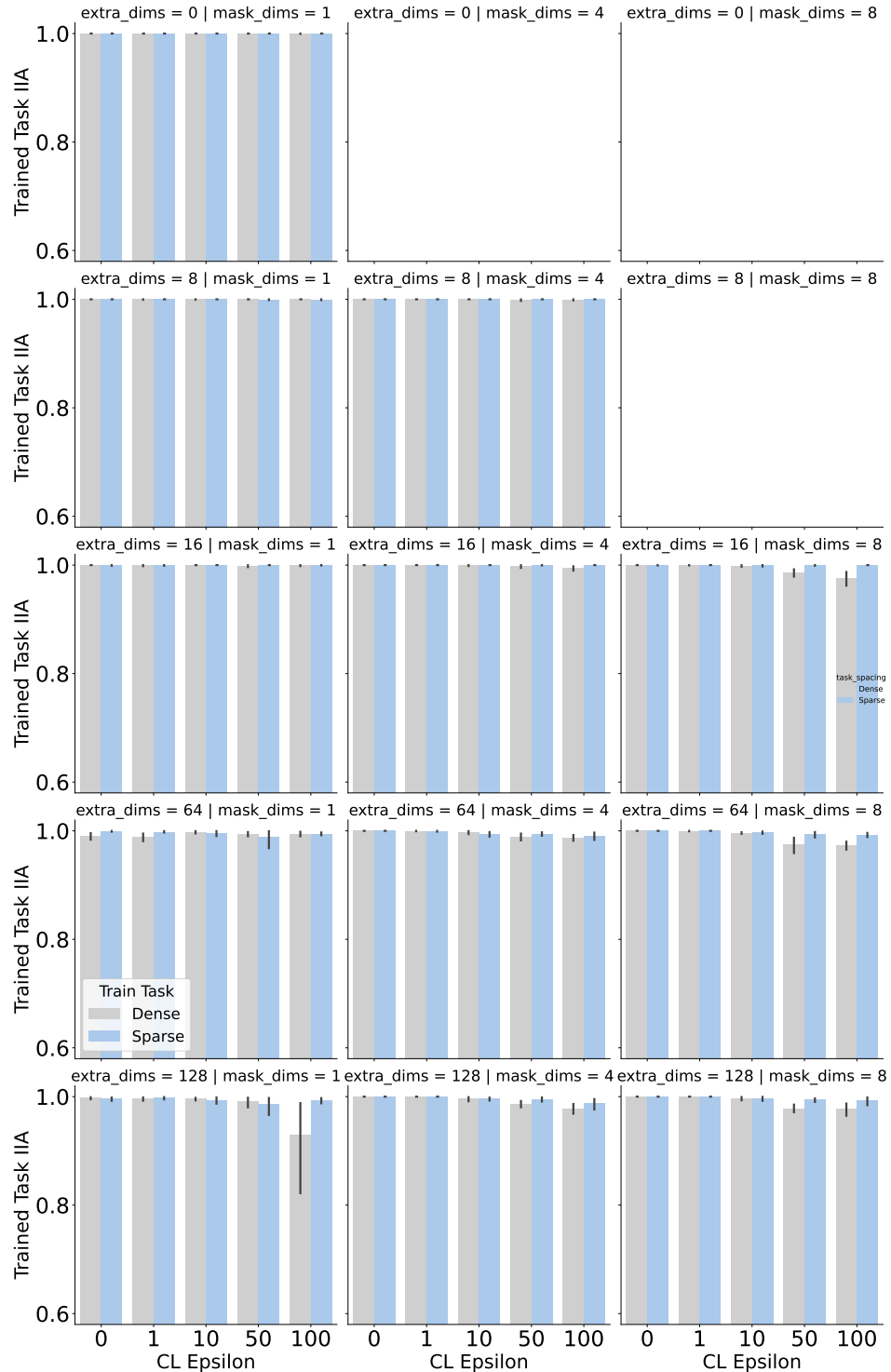


Figure 7: Within distribution hyperparameter search showing the DAS IIA on validation data for the trained task partition. We see the DAS mask dimensions (mask_dims) and extra concatenated noisy input dimensions (extra_dim) across the panel columns and rows. All reported values include the behavioral loss with different values of the CL Epsilon (shown on the x-axis).

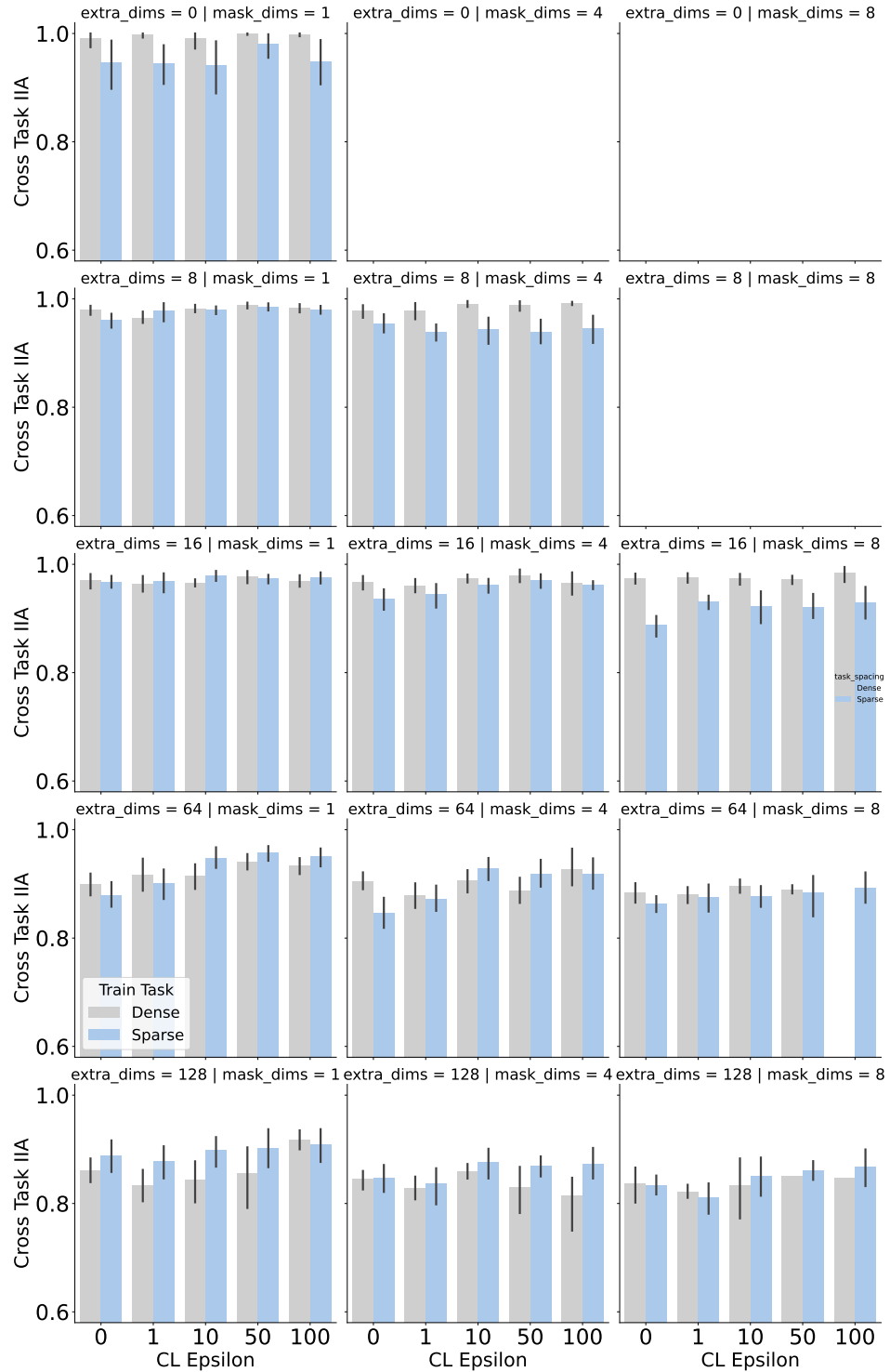


Figure 8: OOD hyperparameter search showing the DAS IIA on validation data for the held-out partition. We see the DAS mask dimensions (mask_dims) and extra concatenated noisy input dimensions (extra_dim) across the panel columns and rows. All reported values include the behavioral loss with different values of the CL Epsilon (shown on the x-axis).

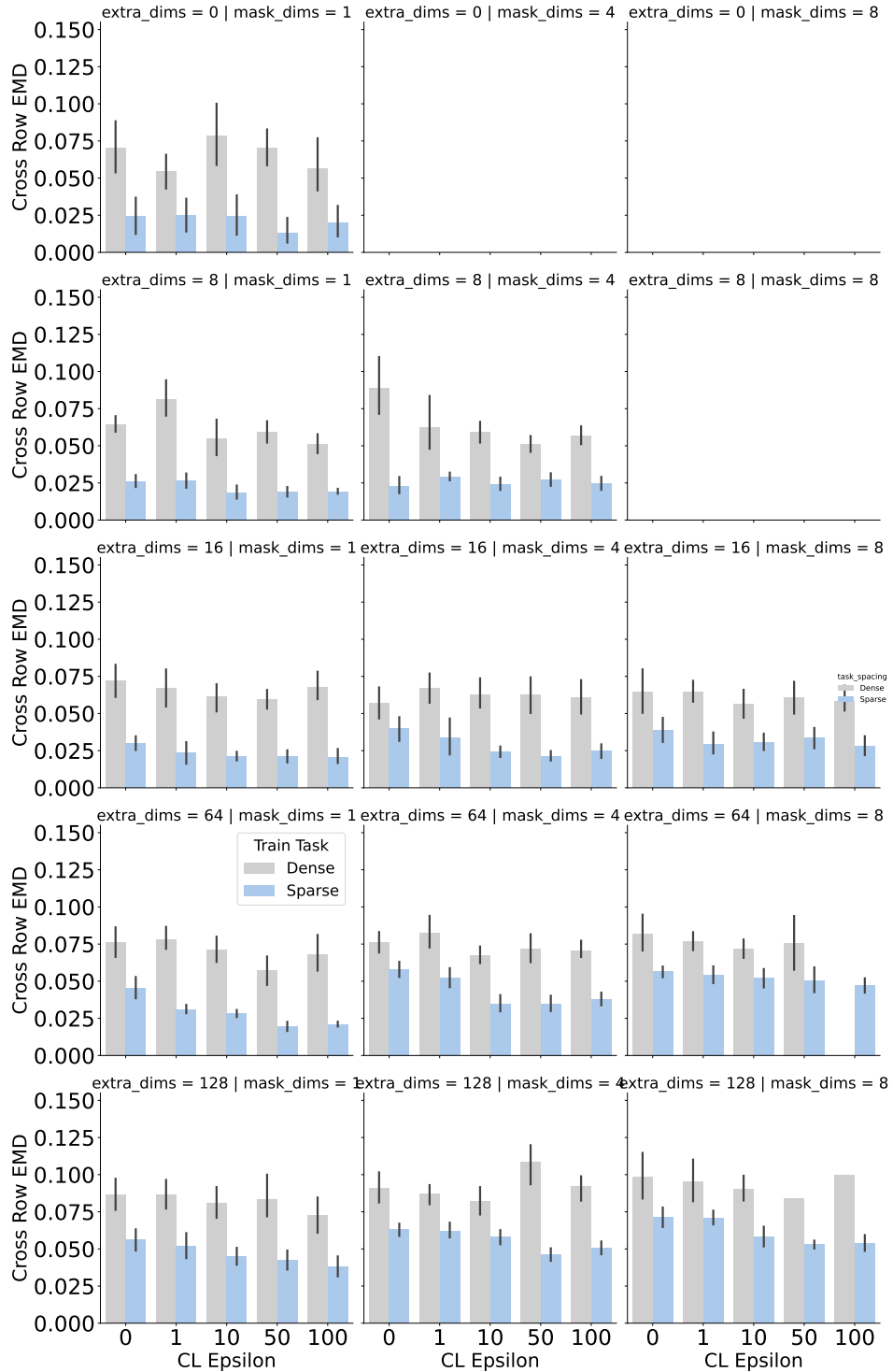


Figure 9: OOD hyperparameter search showing the intervened EMD along causal dimensions only on validation data for the held-out partition. We see the DAS mask dimensions (mask_dims) and extra concatenated noisy input dimensions (extra_dim) across the panel columns and rows. All reported values include the behavioral loss with different values of the CL Epsilon (shown on the x-axis).

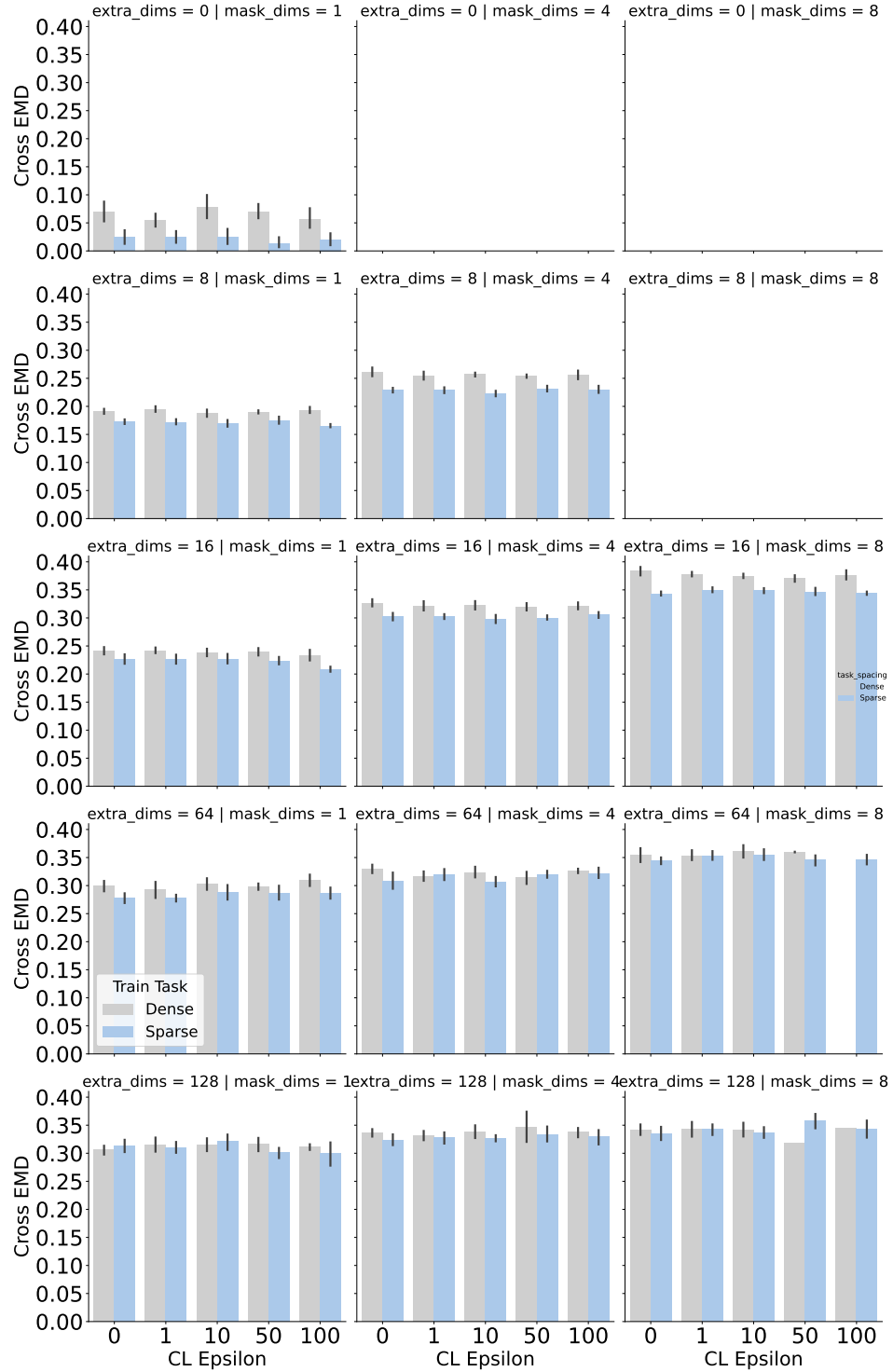


Figure 10: OOD hyperparameter search showing the intervened EMD along all representational dimensions on validation data for the held-out partition. We see the DAS mask dimensions (`mask_dims`) and extra concatenated noisy input dimensions (`extra_dim`) across the panel columns and rows. All reported values include the behavioral loss with different values of the CL Epsilon (shown on the x-axis).